Science World Journal Vol. 20(No 1) 2025 https://dx.doi.org/10.4314/swj.v20i1.2
www.scienceworldjournal.org
ISSN: 1597-6343 (Online), ISSN: 2756-391X (Print)
Published by Faculty of Science, Kaduna State University

Full Length Research Article

FIRST PRINCIPLES STUDY OF STRUCTURAL STABILITY, ELECTRONIC AND MECHANICAL PROPERTIES OF LITHIUM DOPED CALCIUM HYDRIDES AS SUPERCONDUCTORS

*Abdullahi Danlami, Sadiq Garba Abdu, Alhassan Shuaibu and Ismail Magaji

Department of Physics, Faculty of Physical Sciences, Kaduna State University, Kaduna

*Corresponding Author Email Address: abdullahidanlami2020@gmail.com

ABSTRACT
Alkaline earth metal with Hydrogen-rich compounds hold promise as high-temperature superconductors under high pressures. Recent theoretical hydride structures on achieving high-pressure superconductivity are composed mainly of H_2 fragments. Through a systematic investigation of Ca hydrides with different hydrogen contents within both theoretical and experimental methods has become a major research area. In this work we used Density functional theory (DFT) coupled with some Quantum and classical theories to investigate the structural, Mechanical, electronic and superconducting properties of single Lithium atom doped CaH_3 ($Ca_{1-x}Li_xH_3$). Our results show that both pure and Li doped are mechanically stable at 0 pressure with anisotropic structure. In terms of electronic properties both compounds show a metallic nature. Our theoretical calculated T_C are 1.18 K and 2.06 K for CaH_3 and $Ca_{1-x}Li_xH_3$ respectively at 0Gpa, indicating that even calcium hydride with H_3 can possibly be a superconductor.

Keywords: Calcium Hydride (CaH3), Density functional theory, Mechanical and Superconducting properties, Quantum Espresso.

INTRODUCTION

Because of its anticipated exotic features, particularly the expected high-T_c superconductivity in its molecular or atomic form, possibly above room temperature, metallic hydrogen (Wang, et al, 2012) has emerged as the goal in high-pressure physics (Shao, et al, 2019; Ma, et al, 2022). Though metallic hydrogen has been successfully formed in diamond anvil cells at static pressures near 400 GPa (Shao, et al, 2019), according to recent reports, the results are still unverified and up for controversy (Li, et al, 2007; An, et al, 2024). However, Ashcroft's suggestion (Ashcroft, 2004) to exert chemical pressure in hydrogen-rich compounds by adding heavier elements has proven to be particularly successful in lowering the metallization pressure of hydrogen. A wide range of possible candidate materials have been identified through theoretical studies based on structural research and ab initio calculations. These materials include lithium (Guillaume, et al, 2011), scandium (Tse, J. S. 2020).), sulfur (Baettig, P., & Zurek, E. (2011).), and phosphorus hydrides (Wang, et al, 2010), as well as calcium, lanthanum, and yttrium hydrides (Ma, et al, 2004; Konishi, & Naka, N2021) with extremely high hydrogen content.

In the meantime, high-pressure investigations have revealed the presence of high-Tc hydride molecules in at least three chemical systems: PHx (Ma, et al, 2022), LaHx (Talantsev, 2020), and SHx (eng, N., Bi, T., & Zurek, E. (2022). Regarding the latter, compression of SH_2 up to 250 GPa (Sun, et al, 2022) has shown two different superconductivity regimes: a high-Tc phase (203 K), which is the highest confirmed superconducting transition temperature to date, and a low-T_c phase (33–150 K). Depending on the synthesis conditions, different superconducting states emerge. The low-Tc regime is thought to originate from CaH_2 and its potential mixture with CaH_3 to form (intermediate) "Magn´eli"-type structures (Lv, Wang, Zhu, & Ma, 2011), while the high-Tc phase is thought to originate from pure CaH_3 in annealed samples (de Oliveira, 2022)

In accordance with available experimental evidence and crystal structure prediction (CSP) predictions (Papaconstantopoulos, Mehl, & Economou, 2023), the structure of this CaH_3 phase possesses a bcc lattice with Im3m symmetry and is stable at pressures above roughly 150 GPa. Eliashberg theory predicts values of Tc that closely match experimental findings (Papaconstantopoulos, Mehl, & Economou, 2023). CaH_3 is confirmed to be a typical, phonon-mediated superconductor by this outstanding agreement between theory and experiment, as well as by isotope effect measurements (Li, et al, 2024) and recent optical spectroscopy studies. The ability of ab initio calculations to precisely characterize the intriguing features of CaH_3 has made this system a platform for exploring novel concepts that may improve its properties even more.

To find trends that would raise the T_c, Ferreira, et al. (Ferreira, et al, 2024) substituted other metals, such as Alkali earth metal (Mg, Ca, and Be), for the S atoms using the virtual crystal approximation. They discovered that a partial substitution of Ca with Li might raise the value of Tc. suggested doping CaH_3 with elements from adjacent groups in the periodic table and found that in $Ca_{0.925}Li_{0.075}H_3$, a T_c of up to 280 K could be attained at 250 GPa. Recently, Cerqueira et al. (Cerqueira, Sanna & Marques, 2024).) carried out CSP calculations at a fixed composition of $Ca_{0.5}Li_{0.5}H_3$, discovering that the cubic CaH_3 lattice's many decorations correspond to the lowest enthalpy structures. Their electron-phonon calculations indicate that the superconducting temperature drops when Ca is substituted with suggested doping CaH_3 with elements from adjacent groups in the periodic table and found that in $Ca_{0.925}Li_{0.075}H_3$, a T_c of up to 280 K could be attained at 250 GPa. Some few years back, (Jaroń, Grochala, & Hoffmann, 2006) carried out calculations at a fixed composition of Ca and H, discovering that the cubic CaH_3 lattice's many decorations do, in fact, correspond to the lowest enthalpy structures. The scientists explain the drop in the superconducting temperature when Li replaces Ca to a weakening of the covalent H–Ca or H–Li bonds, based on their electron-phonon simulations.

The idea that "recompressed" H_2 in dense hydrogen-dominant hydrides may yield a high Tc is what drives current research on the hydrides of basic elements at high pressures (Duan, et al, 2017;

Zhang, Zhao, & Yang, 2022). Superconductivity has been observed in SiH_4 (Yao, et al, 2007); however, models regarding the origin of superconductivity and the structure of the superconducting state are controversial (Cartwright, N1999; Pellegrini, & Sanna, 2024). A common characteristic of many theoretical structures with predicted T_c values ranging from 10 to 139 K (Pellegrini, & Sanna, 2024) is the ubiquitous presence of molecular hydrogen fragments, except for LuH_3 (Tresca, et al, 2024), where superconductivity was predicted but not observed.

Introduction of an electronegative element, as was demonstrated in the case of K–Ag, increases the ability of the electronegative Ag atoms to accommodate electrons from K into the outermost 5s and 5p valence shells, thereby forming a bonding network and stabilizing the alloy structures that otherwise would not be observed under ambient pressures. At high pressures, unfavorable electron–electron repulsion in the atomic valence shells can be reduced by migration and localization in the empty interstitial regions. It has been observed that the creation of new metallic lithium- or sodium-hydride alloys could result from the transfer of charge from lithium or sodium to hydrogen molecules at high pressures (Fohlmeister, & Stasch, 2015; Marqueño, et al, 2024). The structures are made of monoatomic hydrogen or "predissociated" molecular H_3, depending on the stoichiometry. Hence, the aim of this work is to study the structural stability; electronic and mechanical properties of Lithium (Li) doped Binary calcium hydrides CaH_3.

COMPUTATIONAL DETAILS

Ab-initio calculations within the density functional theory (DFT) as implemented in Quantum ESPRESSO code (Giannozzi, et al, 2009) has been carried out on pure CaH_3, and Li doped CaH_3. The starting crystal parameter was obtained from online data base with CaH_3 in cubic structure in $Fm\bar{3}m$ [225] space group and lattice parameter. For the doping process a simple cell having 16 atoms per unit cell, (4 calcium (Ca) and 12 hydrogen (H) atoms) was used. One Ca atom was replaced with one Li atom which corresponds to 6.2% doping concentration. For structural optimization and electronic properties (Band structure and Density of state) calculations, we have used generalized gradient approximation in the Perdew, Burke, and Ernzerhof (GA-PBE) as exchange correlation functional (Perdew, Kurth, Zupan, & Blaha, 1999; Hammer, Hansen, & Nørskov,1999). kinetic energy cutoff of 40Ry was used and Monkhorst−Pack k-points grid (Monkhorst, & Pack, 1976) of 6 × 6 × 1 was used for sampling in the first Brillouin zone during geometry optimizations of pure and Li doped CaH_3 respectively. All the atoms were fully relaxed until residual force and energy were converged to 0.005 eV/ Å and 10^{-6} eV, respectively.

Mechanical Properties

Analysis of elastic constants (C_{ij}) is essential for understanding the mechanical properties of the materials (Hill, 1952). These constants can be calculated for anisotropic cubic materials by solving the compliance matrix given by

$$C_{ij} = \begin{pmatrix} C_{11} & C_{12} & C_{12} & & & \\ & C_{11} & C_{12} & & & \\ & & C_{11} & & & \\ & & & C_{44} & & \\ & & & & C_{44} & \\ & & & & & C_{44} \end{pmatrix} \quad (1)$$

These constants vary from one crystal system to another based on the respective point groups and Born stability conditions (1). For The materials which are in Cubic the mechanical stability criteria are

$$C_{11} - C_{12} > 0., C_{11} + 2C_{12} > 0, \text{and } C_{44} > 0. \quad (2)$$

Similarly, for the bulk and shear moduli these constants are related within Voight, Reuss and Hill Averaging schemes by the following expressions

Voight Average schemes (Voigt, 1928)

$$B_V = \frac{(C_{11}+2C_{12})}{3} \quad (3)$$

$$G_V = \frac{C_{11}+2C_{12}+3C_{44}}{5} \quad (4)$$

Reuss Average schemes (Reuss, 1929)

$$B_R = B_V \quad (5)$$

$$G_R = \frac{5C_{44}(C_{11}-C_{12})}{4C_{44}3(C_{11}-C_{12})} \quad (6)$$

Hill Average schemes (Hill, 1952)

$$B_H = \frac{1}{2}(B_V + B_R) \quad (7)$$

$$G_H = \frac{1}{2}(G_V + G_R) \quad (8)$$

Young's modulus (E) and Poisson's ratio (σ) can be calculated by using Hill's elastic moduli (B_H) and (G_H), which are given as:

$$E = \frac{9B_HG_H}{3B_H+G_H} \quad (9)$$

$$\sigma = \frac{3B_H-2G_H}{2(3B_H+G_H)} \quad (10)$$

Using thermo_pw code interfacing with QE, the elastic constants in equation 2 of both pure and doped system will be calculated, subsequently; using equations 3 to 10 other mechanical properties will be calculated.

Superconducting Properties

Electron-phonon coupling constant is needed to calculate accurate superconducting transition temperature. The electron-phonon coupling constant can be derived by the estimate equation (Ram, et al. 2012).

$$\lambda = \frac{\gamma_{exp}}{\gamma_{cal}} - 1 \quad (11)$$

The Coulomb repulsion pseudo-potential can be calculated by the following equation (Islam, et al. 1997).

$$\mu^* = 0.26\frac{N(E_F)}{1+N(E_F)} \quad (12)$$

Here, $N(E_F)$ refers the total density of states at the Fermi level. If the result of μ^* stays in the area 0.1 to 0.15, this is regarded as physically reasonable (Kushwaha, et al. 2014).

The $N(E_F)$can be calculated from the TDOS at the Fermi level (Ram, et al. 2012).

$$\gamma_{Cal} = \frac{\pi^2 K_B^2 N(E_F)}{3} \quad (13)$$

Hence the Fermi energy $N(E_F)$ exhibits slight variation with the developing applied stress.

The T_C can be derived by the following McMillan formula (Carbotte, 1990).

$$T_C = \frac{\theta_D}{1.45}\exp\left[-\frac{1.04(1+\lambda)}{\lambda-\mu^*(1+0.62\lambda)}\right] \quad (14)$$

In this here, $\mu*$ refers the Coulomb repulsion pseudo-potential and λ is the electron phonon coupling constant. The λ = $N(E_F)$ V_{e-ph} indicating the electron-phonon interaction energy responsible for the Fermi surface instability and eventual Cooper pairing. It is observed by W. Pickett *et al.* that T_C is climbed according to the raising coupling strength and in this case, every parameter must be equal (Warren & Mikhail, 2019). If the fixed value of λ, T_C is linearly correlated with θ_D. The Debye temperature (θ_D) is accounted for via several methods. In

Science World Journal Vol. 20(No 1) 2025 https://dx.doi.org/10.4314/swj.v20i1.2
www.scienceworldjournal.org
ISSN: 1597-6343 (Online), ISSN: 2756-391X (Print)
Published by Faculty of Science, Kaduna State University

this work, θ_D is calculated with elastic modulus and is the best methods evaluate θ_D [54]. The Debye temperature, $\theta_D$can be calculated by the following equation (Hadi, et al. 2018).

$$\theta_D = (h/K_B)[(3n/4\pi)(N_A\rho/M)]^{1/3}V_m \quad (15)$$

Herein, h is the plank constant, K_B refers the Boltzmann constant, N_A is called the Avogadro number, M identifies the molecular weight, and n is the number of atoms per unit cell.
The V_m is calculated with the help of estimated equation

$$V_m = \left[\left(1/v_l^3 + 2/v_t^3\right)/3\right]^{-\frac{1}{3}} \quad (16)$$

Where, v_l and v_t are the longitudinal as well as transverse sound velocities, respectively. The v_l and $v_t$can be calculated via estimated equation

$$v_l = \left[(3B + 4G)/3\rho\right]^{\frac{1}{2}} \quad (17)$$

$$v_t = \left[(G)/\rho\right]^{\frac{1}{2}} \quad (18)$$

The melting temperature Tm is calculated with the help of elastic constants via the estimate equation (Clerke, 2023).

$$T_m = 354 + 2\left(\frac{2C_{11}+C_{33}}{3}\right) \quad (19)$$

Note that all our calculated values for both pure and doped system are tabulated in chapter four. The summary of all the steps in flow chart is given below.

RESULTS AND DISCUSSION

Structural Stability

Figure 1 (a) and (b) shows our optimized structures of pure CaH_3 and $Ca_{1-x}Li_xH_3$ respectively. The optimized parameters compared with some available literatures are given in Table 1. From Figure 1 (a) It's observed that Ca atom is bonded to six equivalent H atoms to form a mixture of distorted edge and corner-sharing of 3D Crystal alpha bismuth trifluoride structure like, also the (Ca - Ca) bond lengths is found to be around 3.7309 Å. This result agrees with that of (Wang et al, 2012). While in $Ca_{1-x}Li_xH_3$ (Ca - Ca) bond lengths decrease to 3.6869 Å. This decrease is probably due to the small atomic radii of the lithium impurity atom when compared to that of the host Ca atom. More significantly, the present of Li impurity did not change the alpha bismuth trifluoride structure like, although a little defect (d_i) has been observed. Hence, we calculate the defect formation energy $E_{d/form}$, which is the amount of energy change on breaking the bonds of one atom with its ligands in the parent material (pure CaH_3) and forming new bonds with ligands in the reference system (doped $Ca_{1-x}Li_xH_3$) (Cheng et al, 2020).

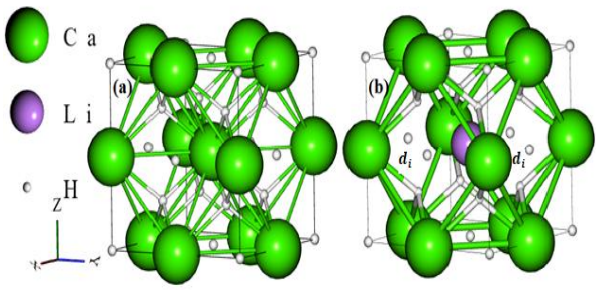

Figure 1 Optimized crystal structures (a) pure CaH_3 (b) $Ca_{1-x}Li_xH_3$

The vacancies of formation energy can be calculated using the following equation.

$$E_{d/form} = E_{Ca_{1-x}Li_xH_3} + E_{CaH_3} + n(\mu_{Ca} + \mu_{Li})$$

Where $E_{Ca_{1-x}Li_xH_3}$ is the energy of the doped system with a given defect, E_{CaH_3} is the energy the pure CaH_3, μ_{Ca} is the chemical potential of Ca and μ_{Li} is the chemical potential of Li. Note that, if the defect is due to an interstitial single atom, $n = 1$. Hence, in Ca rich conditions, $\mu_{Ca} = E_{Ca}$, where E_{Ca} is the energy of bulk stable Ca, and $\mu_{Li} = E_{Li}$, where E_{Li} is the energy of bulk stable Li. Therefore, our computed defect formation energy is about -0.452 eV/atom. Due to the lack of actual experimental value and having negative energy, our result indicates that the doped system is thermodynamically stable at zero pressure and may be favorable for laboratory synthesis. To father investigate the thermodynamic stability of both pure CaH_3 and $Ca_{1-x}Li_xH_3$ we evaluate the mechanical properties of the two compounds as described in chapter three.

Mechanical properties

For the mechanical properties, using thermo_pw code interfacing with QE as mentioned in chapter three, the elastic constants and other mechanical properties for both CaH_3 and $Ca_{1-x}Li_xH_3$ system has been obtained, and tabulated in Table 1.

Table 1: Calculated values of the elastic constants C_{ij}(GPa), bulk modulus B (GPa), shear modulus G (GPa), Young's modulus E (GPa), Poisson's ratio σ, anisotropy factor A and B/G of both CaH_3 and $Ca_{1-x}Li_xH_3$ compounds.

Material	C_{11}	C_{12}	C_{44}	B	G	E	σ	A	B/G
CaH_3(this work	162.45	92.22	66.41	115.63	109.22	142.01	0.295	1.89	1.05
$Ca_{1-x}Li_xH_3$ (this work	170.12	102.01	77.03	1251	121.04	156.74	0.290	2.26	1.03
[a]SH_3	191.40	103.50	61.30	116.40	640	146.30	0.35	1.09	0.44

Science World Journal Vol. 20(No 1) 2025 https://dx.doi.org/10.4314/swj.v20i1.2
www.scienceworldjournal.org
ISSN: 1597-6343 (Online), ISSN: 2756-391X (Print)
Published by Faculty of Science, Kaduna State University

Since the bulk modulus is usually assumed to be a measure of resistance to volume change by applied pressure. From Table 1, the value of the bulk modulus for both CaH_3 and $Ca_{1-x}Li_xH_3$ compounds are larger, indicating that the compounds have a strong resistance to volume change by applied pressure. The two constants E and G, are all that are needed to fully characterize the stiffness of an isotropic material. The present calculated results of these moduli demonstrate that the both CaH_3 and $Ca_{1-x}Li_xH_3$ compound are stiff. Poisson's ratio (σ) defined as the ratio of transverse strain to the longitudinal strain is used to reflect the stability of the material against shear and provides information about the nature of the bonding forces. It takes the value: $-1 < \sigma < ½$. No real material is known to have a negative value of σ. So, this inequality can be replaced with $0 < \sigma < ½$. The low value of Poisson's ratio indicates a large compression of volume and when $\sigma = 0.5$ no volume change occurs. Bigger the Poisson's ratios, the better the plasticity. The present calculated result of Poisson's ratio shows that both the CaH_3 and $Ca_{1-x}Li_xH_3$ intermetallic compound are of good plasticity with $Ca_{1-x}Li_xH_3$ as higher. The σ =0.25 and σ= 0.5 are the lower limit and upper limit for central forces in solids, respectively. The obtained value of Poisson's ratio (s) of both CaH_3 and $Ca_{1-x}Li_xH_3$ are larger than the lower limit value (σ = 0.25), which indicates that the interatomic forces of both CaH_3 and $Ca_{1-x}Li_xH_3$ are central forces.

The Zener anisotropy factor (A) is a measure of the degree of anisotropy in solid (Zener, 1948). It takes the value of 1 for an isotropic material. It provides a measure of the degree of elastic anisotropy, when the values A are smaller or greater than unity. The Zener anisotropy factor (A) of both CaH_3 and Ca1-xLixH3 compound is calculated by the following equation:

$$A = \frac{2C_{44}}{C_{11}-C_{12}} \qquad (20)$$

As shown in Table 1, that the calculated Zener anisotropy factor A is larger than 1 for both Compounds that are elastically anisotropic materials.

The ratio B/G is a simple relationship related to the brittle or ductile behavior of materials. It has been proposed by Pugh (Pugh,1954). A high B/G ratio is associated with ductility, whereas a low value corresponds to the brittleness. The critical value separating ductile and brittle material is 1.75. The calculated results are listed in Table 1. In this work, the obtained results of both compounds indicate that they can be classified as ductile materials at zero pressure. Another parameter indicating the brittleness or ductility of the material is the Cauchy relation defined as: $C_P = C_{11} - C_{12}$. The material is expected to be ductile, if the value of this expression is positive, on the other hand, if its value is negative, the material is brittle (Pettifor, 1992). At zero pressure, we found 31.89 GPa and 261 GPa for Cauchy pressure of CaH_3 and $Ca_{1-x}Li_xH_3$ respectively. From these values and according to the above criterion, the studied compounds are said to be ductile. Thus, the ductile nature of CaH3 and $Ca_{1-x}Li_xH_3$ compound can be related to a metallic character in their bonds.

To demonstrate the elastic anisotropy and the stiffness of these materials, the variation of Young's modulus, and shear modulus were considered. With an intention to explore this anisotropic and stiffness nature, we have estimated the 3D of Y and G, for CaH_3 and $Ca_{1-x}Li_xH_3$ using XCrysdeen as shown in Figure 2 and 3 respectively.

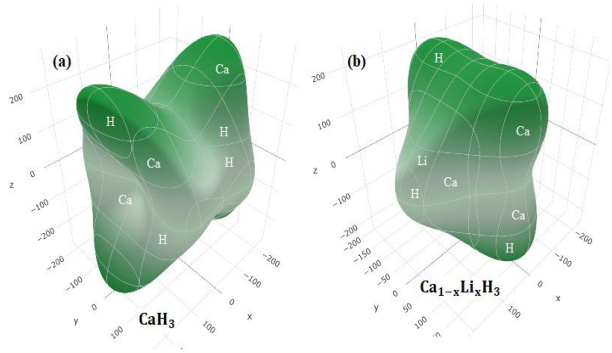

Figure 2: Three-dimensional (3D) plot of Young's modulus(Y) for (a) CaH_3 and (b) $Ca_{1-x}Li_xH_3$

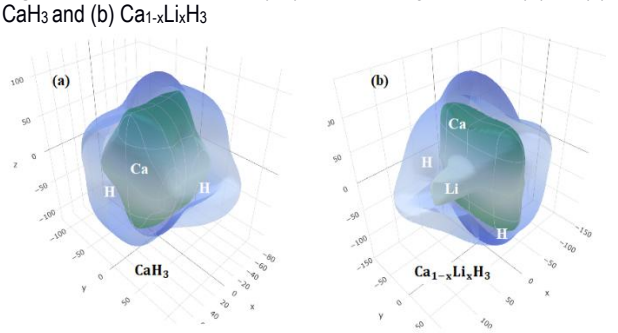

Figure 3: Three-dimensional (3D) plot of Shear modulus (G) for CaH_3 and $Ca_{1-x}Li_xH_3$

From the two plots, it has been observed that they have similar mechanical anisotropy except the slight differences in the magnitude in both Y and G. Considering Figure 2(a) the 3D representation of Y for CaH_3 indicating that the Y is more anisotropic in xy planes. The least anisotropy is observed in the xz plane in which the maximum values are at an angle of 45° between the vertical and horizontal axes. The extent of anisotropy for yz planes is midway between those in the xy and xz planes in which the maximum is on the vertical axis.

Interestedly, when Li atom impurity is introduced, the 3D representation of Y for $Ca_{1-x}Li_xH_3$ Figure 2(b) indicates that the Y still has more anisotropic in xy planes only with increases in magnitude and having the maximum values are at an angle opposite of 45° between the vertical and horizontal axes.

Similarly for the case of share modulus G as shown in Figure 3. From Figure 3(a) the 3D representation of G for pure CaH_3 indicating that the G is more anisotropic in xy planes. The least anisotropy is observed in the xz plane in which the maximum values are at an angle of 45° between the vertical and horizontal axes. The extent of anisotropy for yz planes is midway between those in the xy and xz planes in which the maximum is on the vertical axis.

Interestedly, when Li atom impurity is introduced, the 3D representation of G for $Ca_{1-x}Li_xH_3$ Figure 2(b) indicates that the G still has more anisotropic in xy planes only with increases in magnitude and having the maximum values are at an angle opposite of 45° between the vertical and horizontal axes.

Electronic Properties

Electronic Properties of pure CaH_3

To understand the electronic behavior in pure CaH_3, we calculate the electronic band structure within a high symmetry Brillouin zone (Γ → X → M → Γ), the density of state (DOS) and projected density of state (PDOS) within a DFT-GGA as depicted in Figure 3. From the plot, it

Science World Journal Vol. 20(No 1) 2025 https://dx.doi.org/10.4314/swj.v20i1.2
www.scienceworldjournal.org
ISSN: 1597-6343 (Online), ISSN: 2756-391X (Print)
Published by Faculty of Science, Kaduna State University

has been observed that, there are bands near the Fermi level (located at 0) which are probably the d bands of the metal Ca. Although there is some difference between bands at the Γ point in the conduction band, but still there is no significant crystal field splitting. As can be incidental from the plot, these bands are quite similar in the other metal hydride. The lowest band in the valance band shows the characteristic of free-electron-like behavior near the Γ point and crosses into the d bands indicating a metallic nature. This free electron band from the Ca atom hybridizes with the H s orbital, forming a bonding band which has shifted down in energy, this kind of band possesses significant H-s character as can be seen in the PDOS shown in Figure 47(b).

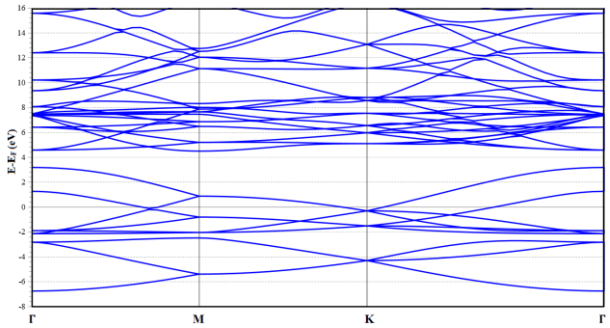

Figure 4: Calculated electronic band structure of pure CaH_3 with DFT-GGA optimized parameters

To get more information on the electronic character in pure CaH_3 the total and partial DOS has been obtained and shown in Figure 5(a) and 5(b) respectively. Figure 5(a) confirmed the metallicity character of pure CaH_3 as observed in the band structure plot. While for the PDOS plot Figure 5(b) it has been observed that the high contributions come from Ca s and p orbitals in both conduction band and balance band region with minimal contribution of H-s orbital. These clearly indicate a possible strong meta-metal bond which one of the requirement for superconducting material, also this for any doping the Ca atom side will be a favorable. Although we have less literature on this metal Hydride with H_3, but still our result shows good agreement with some reported theoretical results. Other Metal Hydride with even number of Hydrogen (CaH_2, CaH_6 and CaH_{12}) has shown similar character.

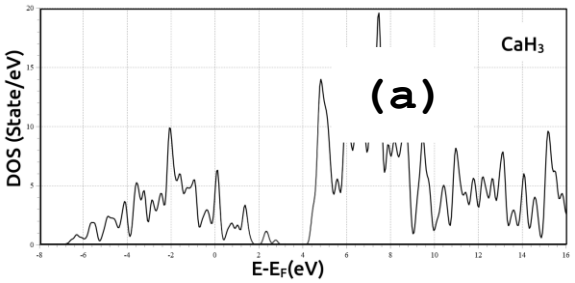

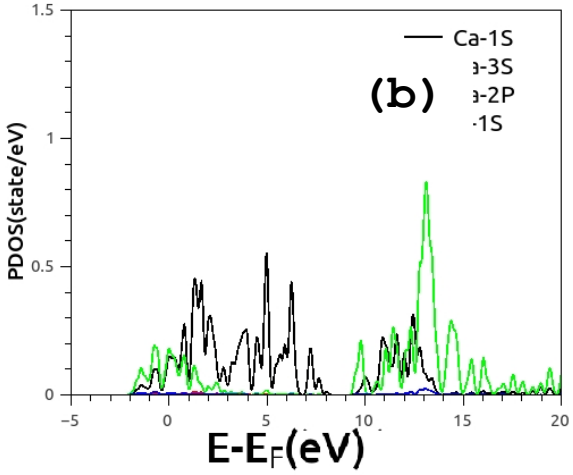

Figure 5: (a) Total density of state pure (DOS) and (b) PDOS for CaH_3 with a DFT-GGA optimized parameters

Electronic properties of $Ca_{1-x}Li_xH_3$

To investigate the effect of Li introduction as impurity on electronic properties, both Band structure, DOS and PDOS of $Ca_{1-x}Li_xH_3$ have been evaluated and shown in Figure 6 and Figure 8 (a) and (b) respectively.

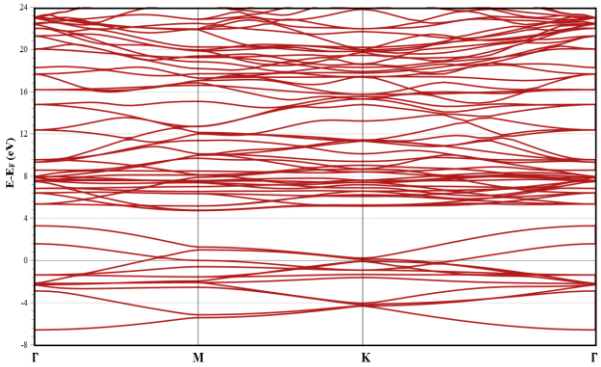

Figure 6: Calculated electronic band structure of $Ca_{1-x}Li_xH_3$ with DFT-GGA optimized parameters

From Figure 6, it has been observed that that $Ca_{1-x}Li_xH_3$ has similar ban structure with that of pure CaH_3, having a metallic nature. But the presence of Li impurity induced more conductivity as indicated in the conduction band at the energy range between 5eV to 8eV. More significantly, the number of overlapping bands at the Fermi level (coincide at 0eV) has significantly increased indicating that magnetic moment can probably be induced due to the presence of Li impurity. Similarly, the possibility of a superconductive nature is paramount. This result agrees with the results for AlH_3 by (Pickard, C. J., & Needs, R. J. (2007).

Figure 8 is the calculated total density of state (DOS) of the $Ca_{1-x}Li_xH_3$ which is also confirmed what is in the band structure. In both cases of the band structure and DOS the Fermi level crosses both conduction and valance bands indicating a strong metallic nature.

Science World Journal Vol. 20(No 1) 2025 https://dx.doi.org/10.4314/swj.v20i1.2
www.scienceworldjournal.org
ISSN: 1597-6343 (Online), ISSN: 2756-391X (Print)
Published by Faculty of Science, Kaduna State University

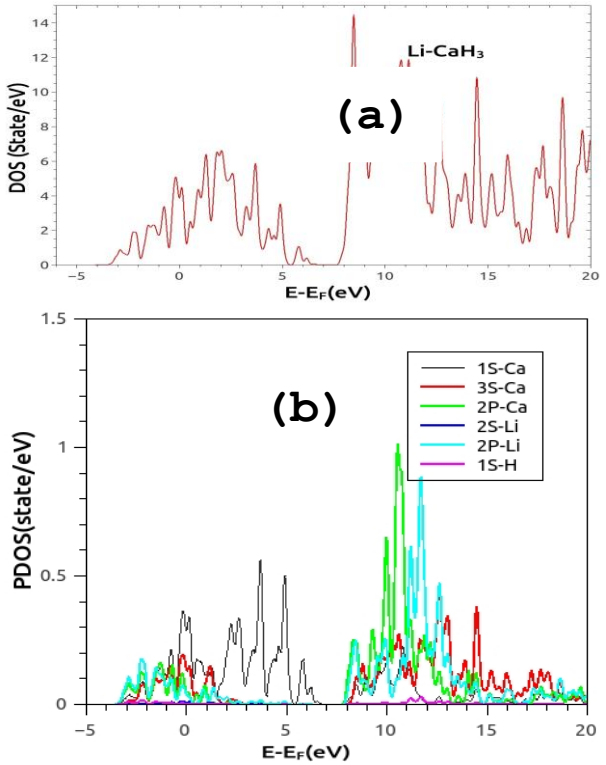

Figure 8: Calculated (a) TDOS and (b) PDOS of $Ca_{1-x}Li_xH_3$ with DFT-GGA optimized parameters

Superconducting Properties

To find out about the superconducting nature of both systems, all required properties as described in chapter three have been evaluated and tabulated in Table 2. Despite it's well known that at 0 GPa, the theoretically calculated value of θ_D is smaller than that of experimental result in all material, we emphasized that our results would serve as prediction for these materials.

Table 2: Calculated results of density ρ(g/cc), sound velocities v_l , v_t, V_m (m/s), Debye temperature θ_D (K) and melting temperature T_m (K) of CaH_3 and $Ca_{1-x}Li_xH_3$ at 0 GPa,

Compound	ρ	v_l	v_t,	V_m	θ_D	T_m
CaH_3	3.33	4422.5	1121.23	1652.16	102.05	986.6
$Ca_{1-x}Li_xH_3$	36	5238	2101.45	1982.23	150.33	1232.6

As mentioned earlier, T_C can be obtained using McMillan formula given in Equation 3.15. Hence our theoretical calculated T_C are 1.18 K and 2.16 K for CaH_3 and $Ca_{1-x}Li_xH_3$ respectively, although these values are less than those obtained on CaH4 2.69K at 0GPa (Wang et al, 2012), but it's clearly evidence that even Calcium Hydride with H_3 can be a good superconductor. Similarly, since T_C is linearly dependent on with driving pressure, our calculated T_C may increase with driving pressure.

Conclusion

In conclusion, structural, mechanical, electronic and superconducting properties of pure and Lithium doped Calcium Hydride (CaH_3) were studied using DFT-GGA simulations. The structural analysis shows that pure CaH3 is mechanically stable with optimized lattice constants of $a = 3.78$ Å, while instructing the Li atom impurity decreases the lattice parameters and creating a vacancy with defect formation energy is about -0.452 eV/atom showing that $Ca_{1-x}Li_xH_3$ could be thermodynamically, and probably favorable for laboratory synthesis. For the obtained electronic properties, a banstructure and density of states (DOS) shows a metallic nature for both compounds. These findings agree with some metal hydrides of similar structure (LuH_3). Finally, a theoretical calculated T_C of 1.18 K and 2.06 K at 0GPa for CaH_3 and $Ca_{1-x}Li_xH_3$ are observed, showing that both pure and doped systems will be promising candidate as a superconductor.

REFERENCES

Allen, J. W., & Mitrovic, B. (2005). The Fermi surface and electron-phonon interactions in superconductivity. *Journal of Low Temperature Physics, 140*(5–6), 619–632 https://doi.org/10.1007/s10909-005-6282-5

An, D., Duan, D., Zhang, Jiang, Q., Ma, T., Huo, Z., ... & Cui, T. (2024). Type-I calcium hydride and its hydrogen-vacancy structures are at high pressure. *Physical Review B*, *110*(5), 054505.

Ashcroft, N. W. (2004). Hydrogen dominant metallic alloys: high temperature superconductors. *Physical Review Letters*, *92*(18), 187002.

Baettig, P., & Zurek, E. (2011). Pressure-stabilized sodium polyhydrides: NaH n (n> 1). *Physical Review Letters*, *106*(23), 237002.

Baroni, S., Bonini N., Calandra M., et al (2009). QUANTUM ESPRESSO; Modular and Open-source Software project for Quantum simulations of material Journal of Physics. Condensed matter, 21(39), 395502.

Carbotte, J. P. (1990). Properties of boson-exchange superconductors. Rev. Mod. Phys. 62, 1027-157

Cartwright, N. (1999). Models and the limits of theory: quantum Hamiltonians and the BCSmodels of superconductivity. *Ideas in Context*, *52*, 241-281.

Cerqueira, T. F., Sanna, A., & Marques, M. A. (2024). Sampling the materials space for conventional superconducting compounds. *Advanced Materials*, *36*(1), 2307085.

de Oliveira, J. M. N. Q. (2022). *Phase Diagrams of High-Pressure Ternary Systems* (master'sthesis, Universidade de Coimbra (Portugal).

Degtyareva, O., Proctor, J. E., Guillaume, C. L., Gregoryanz, E., & Hanfland, M. (2009). Formation of transition metal hydrides at high pressures. *Solid State Communications*, *149*(39-40), 1583-1586.

Duan, D., Liu, Y., Ma, Y., Shao, Z., Liu, B., & Cui, T. (2017). Structure and superconductivity of hydrides at high pressures. *National Science Review*, *4*(1), 121-135.

Eremets, M. I., Trojan, I. A., Medvedev, S. A., Tse, J. S., & Yao, Y. (2008). Superconductivity in hydrogen dominant materials: Silane. *Science*, *319*(5869), 1506-1509.

Ferreira, P. N., Lucrezi, R., Guilhon, I., Marques, M., Teles, L. K., Heil, C., & Eleno, L. T. (2024). Ab initio modeling of superconducting alloys. *Materials Today Physics*, 101547

Fohlmeister, L., & Stasch, A. (2015). Alkali metal hydride complexes: well-defined molecular species of saline hydrides. *Australian Journal of Chemistry*, *68*(8), 1190-1201.

Gao, G., Oganov, A. R., Bergara, A., Martinez-Canales, M., Cui, T., Iitaka, T., ... & Zou, G. (2008). Superconducting high-pressure phase of germane. *Physical review letters*, *101*(10), 107002.

Gao, G., Wang, L., Li, M., Zhang, J., Howie, R. T., Gregoryanz, E., ... & John, S. T. (2021). Superconducting binary hydrides: Theoretical predictions and experimental progresses. *Materials Today Physics*, *21*, 100546.

Giannozzi, P., Baroni, S., Bonini, N., Calandra, M., et al (2009). Quantum ESPRESSO: Modular

and open-source software project for quantum simulations of material *Journal of Physics: Condensed Matter, 21*(39), 395502.

https://doi.org/10.1088/0953- 8984/21/39/395502

Guillaume, C. L., Gregoryanz, E., Degtyareva, O., McMahon, M. I., Hanfland, M., Evans, S., ... & Mao, H. K. (2011). Cold melting and solid structures of dense lithium. *Nature Physics*, *7*(3), 211-214.

Hadi, M. A., Islam, M. N. & Babu, M. H. (2018). Cubic perovskite Pb (Mg1/3Nb2/3)O3: A damage tolerant, machinable, and thermal barrier coating material, Z. Naturforsch. 74, 71-81

Hammer, B., Hansen, L. B., & Nørskov, J. K. (1999). Improved adsorption energetics within density-functional theory using revised Perdew-Burke-Ernzerhof functionals. *Physical Review B, 59*(11), 7413–7421. https://doi.org/10.1103/PhysRevB.59.7413.

Li, B., Li, Y., Yang, K., Cui, Q., Ma, Y., & Zou, G. (2007). Raman evidence of a new high-pressure phase in calcium hydride. *Journal of Physics: Condensed Matter*, *19*(22), 226205.

Li, X., Guo, Z., Zhang, X., & Yang, G. (2024). Layered Hydride LiH4 with Pressure- Insensitive Superconductivity. *Inorganic Chemistry*, *63*(18), 8257-8263.

Liu, H., Xie, Y., Zheng, L., & Zhao, X. (2013). Effects of calcium doping on the performance of TiO_2 photoanodes in dye-sensitized solar cells. *Journal of Materials Science: Materials in Electronics, 24*(1), 142–147. https://doi.org/10.1007/s10854-012-0929-5.

Lilia, B., Hennig, R., Hirschfeld, P., Profeta, Sanna, A., Zurek, E., ... & Valenti, R. (2022). The 2021 room-temperature superconductivity roadmap. *Journal of Physics: Condensed Matter*, *34*(18), 183002.

Lv, J., Wang, Y., Zhu, L., & Ma, Y. (2011). Predicted novel high-pressure phases of lithium. *Physical Review Letters*, *106*(1), 015503.

Ma, L., Wang, K., Xie, Y., Yang, X., Wang, Y., Zhou, M., ... & Ma, Y. (2022). High-temperature superconducting phase in clathrate calcium hydride CaH 6 up to 215 K at a pressure of 172 GPa. *Physical Review Letters*, *128*(16), 167001.

Ma, Y., Tse, J. S., Cui, T., Klug, D. D., Zhang, L., Xie, Y., ... & Zou, G. (2005). First principles study of electron-phonon coupling in hole-and electron-doped diamonds in the virtual

Hanfland, M., Proctor, J. E., Guillaume, C. L., Degtyareva, O., & Gregoryanz, E. (2011). High-pressure synthesis, amorphization, and decomposition of silane. *Physical ReviewLetters*, *106*(9), 095503. Hill, R., (1956). Proc. Phys. Soc., London, Sect. A 65, p. 349

Islam, A. K. M. A. & Naqib, S. H. (1997). Possible explanation of high Tc in some 2D cuprate superconductors. J Phys. Chem. Solids 58, 1153.

Jain, A., Ong, S. P., Hautier, G., Chen, W., Richards, W. D., Dacek, S., Cholia, S., Gunter, D., Skinner, D., Ceder, G., & Persson, K. A. (2013). The Materials Project: A materials genome approach to accelerating materials innovation. *APL Materials, 1*(1), 011002. https://doi.org/10.1063/1.4812323.

Kafle, P. et al. (2022). Ab initio study of Li-Mg-B Superconductors. ArXiv:2208. 12855v1.

Kokalj A., (1999). XCrySDen- a new program for displaying Crystalline Structures and electron densities. Journal Of Molecular Graphics and Modelling, 17(3-4), 176-179.

Konishi, K., & Naka, N. (2021). Phonon-assisted excitonic absorption in diamond. *Physical Review B*, *104*(12), 125204.

Kushwana, S. K. et al. (2014). Superconducting properties and electronic structure of NaBi. J Phys. Condens. Matter 26, 212201.

Laflamme Janssen, J., Côté, M., Louie, S. G., & Cohen, M. L. (2010). Electron-phonon coupling in C 60 using hybrid functionals. *Physical Review B—Condensed Matter and Materials Physics*, *81*(7), 07 crystal approximation. *Physical Review B—Condensed Matter and Materials Physics*, *72*(1), 014306.

Szczesniak M., Szczesniak R., Durajski A.P., (2023). High-pressure synthesis and superconductivity of Bariumpolyhydride. Journal of superconductivity and novel magnetism 36, 1234-1245.

Monkhorst, H. J., & Pack, J. D. (1976). Special points for Brillouin-zone integrations. *Physical Review B, 13*(12), 5188–5192. https://doi.org/10.1103/PhysRevB.13.5188.

Onnes, H. K; (1911). The superconductivity of mercury. Comm. Phys. Lab. Univ. Leiden, 122, 122-124.

Papaconstantopoulos, D. A., Mehl, M. J., & Economou, E. N. (2023). High temperature superconductivity in the Ca-Sc-H system. *Physical Review B*, *108*(22), 224508.

Pellegrini, C., & Sanna, A. (2024). Ab initio methods for superconductivity. *Nature Reviews Physics*, 1-15.

Perdew, J. P., Burke, K., & Ernzerhof, M. (1996). Generalized Gradient Approximation Made Simple. *Physical Review Letters, 77*(18), 3865–3868.

Pettifor, D.G., (1992). Mater. Sci. Technol. 8 345

Pickett, W. E., Allen, J. W., & Hohenberg, P. (2019). The influence of electron-phonon interactions on superconductivity: Strong coupling in the high-Tc cuprates. *Reviews of Modern Physics*, 91(3), 035001. https://doi.org/10.1103/RevModPhys.91.035001

Pickard, C. J., & Needs, R. J. (2007). High-pressure phases of H_2 and the possibility of superconductivity. Nature Physics, 3(9), 473–476. https://doi.org/10.1038/nphys663.

Pugh, S. F. (1954). Philos. Mag. 45 823.

Ram, S., Kanchana, V., Vaitheeswaran, G., Svane, A., Dugdale, S.B. & Christensen,N.E. Electronic topological transition in LaSn3 under pressure. Phys. Rev.B85 (2012) 174531.

Reuss, A., & Angew, Z., (1929). Math. Mech. 9 49.

Shao, Z., Duan, D., Ma, Y., Yu, H., Song, H., Xie, H., ... & Cui, T. (2019). Unique phase diagram and superconductivity of calcium hydrides at high pressures. *Inorganicchemistry*, *58*(4), 2558-2564.

Sun, Y., Li, X., Iitaka, T., Liu, H., & Xie, Y. (2022). Crystal structures and superconductivity of carbonaceous sulfur hydrides at pressures up to 300 GPa. *Physical Review B*, *105*(13), 134501.

Talantsev, E. F. (2020). Debye temperature in LaHx-LaDy superconductors. *arXiv preprint arXiv:2004.03155*.

Tamblyn, I., Raty, J. Y., & Bonev, S. A. (2008). Tetrahedral clustering in molten lithium under pressure. *Physical review letters*, *101*(7), 075703.

Tresca, C., Forcella, P. M., Angeletti, A., Ranalli, L., Franchini, C., Reticcioli, M., & Profeta, G. (2024). Molecular hydrogen in the N-doped LuH_3 system as a possible path to superconductivity. *Nature Communications*, *15*(1), 7283.

Tse, J. S., Yao, Y., & Tanaka, K. (2007). Novel superconductivity in metallic SnH_4 under high pressure. *Physical review letters*, *98*(11), 117004.

Vasilief, I. *QtiPlot: Data Analysis and Scientific Visualization* [Computer software]. Available from: http://www.qtiplot.com.

Van Voorhis T., Scuseria G.E., (1998). Anovel form for the exchange-correlation energy functional. Journal of Chemical Physics, 109 (2), 400-410.

Voigt, W., (1928). Lehrbuch de Kristallphysik, Terubner, Leipzig.

Wang, H; Tse, J. S; Tanaka, K; Litaka, T; and Ma, Y; (2012). Superconductive sodalite-like clatlike clathrat calcium hydride at high pressures Proc. Natl. Sci. 109 6463-6.

Wang, R. S., Peng, D., Zong, L. N., Zhu, Z. W., & Chen, X. J. (2023). Full set of superconducting parameters of K3C60. *Carbon*, *202*, 325-335.

Wang, Y., Lv, J., Zhu, L., & Ma, Y. (2010). Crystal structure prediction via particle-swarm optimization. *Physical Review B—Condensed Matter and Materials Physics*, *82*(9), 094116.

Wang, J., Chernatynskiy, A., Phillpot, S. R., & Wolf, D. (1997). Elastic stability limits of material as a function of crystal symmetry and anisotropy. *Physical Review B, 55*(4), 2487–2493. https://doi.org/10.1103/PhysRevB.55.2487.

Warren, P. & Mikhail, E. (2019). The quest for room-temperature superconductivity in hydrides. Phys. Today 72, 5-52.

Yalameha, S., Nourbakhsh, Z., & Vashaee, D. (2022). ElATools: A tool for analyzing anisotropicastic properties of the 2D and 3D materials. *Computer Physics Communications, 271* 108195. https://doi.org/10.1016/j.cpc.2021.108195.

Yang X.,Wang, K., Xie, Y.,Wang, H., Liu, G., et al (2021). High-Temperature Superconducting Phase in Clathrate Calcium Hydride CaH_6 up to 215 K at a Pressure of 172 GPa. *Physical Review Letters*, *128*(16), 167001. https://doi.org/10.1103/PhysRevLett.128.167001

Yao Y, Tse JS, Tanaka K, Marsiglio F, Ma Y (2009) Superconductivity in lithium under high pressure investigated with density functional and Eliashberg theory. Phys Rev B 79:054524.

Yao, Y., Tse, J. S., Ma, Y., & Tanaka, K. (2007). Superconductivity in high-pressure SiH_4. *Europhysics Letters*, *78*(3), 37003.

Zhang, X., Zhao, Y., & Yang, G. (2022). Superconducting ternary hydrides under high pressure. *Wiley Interdisciplinary Reviews: Computational Molecular Science*, *12*(3), e1582.

Zener, C., (1948). Elasticity and Anelasticity of Metals, University of Chicago Press, Chicago.